Cloud liquid water path comparisons from passive microwave and solar reflectance satellite measurements: Assessment of sub-field-of-view cloud effects in microwave retrievals

Thomas J. Greenwald

Cooperative Institute for Research in the Atmosphere, Colorado State University, Fort Collins

Sundar A. Christopher and Joyce Chou

Institute of Atmospheric Sciences, South Dakota School of Mines and Technology, Rapid City

Abstract. Satellite observations of the cloud liquid water path (LWP) are compared from special sensor microwave imager (SSM/I) measurements and GOES 8 imager solar reflectance (SR) measurements to ascertain the impact of sub-field-of-view (FOV) cloud effects on SSM/I 37 GHz retrievals. The SR retrievals also incorporate estimates of the cloud droplet effective radius derived from the GOES 8 3.9-μm channel. The comparisons consist of simultaneous collocated and full-resolution measurements and are limited to nonprecipitating marine stratocumulus in the eastern Pacific for two days in October 1995. The retrievals from these independent methods are consistent for overcast SSM/I FOVs, with RMS differences as low as 0.030 kg m^{-2}, although biases exist for clouds with more open spatial structure, where the RMS differences increase to 0.039 kg m^{-2}. For broken cloudiness within the SSM/I FOV the average beam-filling error (BFE) in the microwave retrievals is found to be about 22% (average cloud amount of 73%). This systematic error is comparable with the average random errors in the microwave retrievals. However, even larger BFEs can be expected for individual FOVs and for regions with less cloudiness. By scaling the microwave retrievals by the cloud amount within the FOV, the systematic BFE can be significantly reduced but with increased RMS differences of 0.046-0.058 kg m^{-2} when compared to the SR retrievals. The beam-filling effects reported here are significant and are expected to impact directly upon studies that use instantaneous SSM/I measurements of cloud LWP, such as cloud classification studies and validation studies involving surface-based or in situ data.

1. Introduction

Presently, space-borne passive sensors are capable of observing the liquid water path (LWP) of clouds over land and water from two distinct methods. The first method makes use of reflected solar radiation measurements at nonabsorbing visible (0.5-0.7 μm) and water-absorbing near-infrared (3.7-3.9 μm) wavelengths to determine the cloud visible optical depth and the effective radius of the cloud droplets [*Nakajima and King*, 1990; *Han et al.*, 1994]. From these quantities the cloud LWP is inferred. The second approach, which is applied mainly over water surfaces [e.g., *Petty*, 1990; *Greenwald et al.*, 1995] and has had some success over land as well [*Jones and Vonder Haar*, 1990; *Greenwald et al.*, 1997], is more direct and uses measurements at microwave frequencies ($\approx$18-85 GHz) to retrieve cloud LWP, independent of the drop size.

Since validating these methods is often very difficult because of a lack of in situ or ground measurements, another way to test these independent methods is to compare them directly. Indeed, identifying the conditions under which these methods agree or disagree can provide insight into the uncertainties and limitations in the retrievals. This knowledge is crucial for future instrument

platforms, such as the Earth Observing System (EOS), which will include a suite of multispectral sensors to make it possible to apply both methods for the global monitoring of cloud properties from space for climate studies [*Wielicki et al.*, 1995].

As yet, few investigations have attempted to compare these two types of methods. One of the earliest studies [*Lojou et al.*, 1991] used spatially averaged cloud LWPs retrieved from GOES 1 visible infrared spin scan radiometer (VISSR) and scanning multichannel microwave radiometer (SMMR) measurements for selected cases over the Indian Ocean. There was satisfactory agreement between the methods; however, the impact of ice particles (the study was not restricted to water clouds) and precipitating clouds on the comparisons is uncertain. Two other studies that followed, *Greenwald et al.* [1993] and *Lin and Rossow* [1994], were confined to nonprecipitating marine stratocumulus but were rather limited. In each of the previous studies either a constant effective radius was assumed or the *Stephens* [1978] parameterization was used in the solar reflectance (SR) retrievals. These assumptions and approximations introduce further, usually small, uncertainties in the retrievals.

One issue that has been largely unexplored is the influence of sub-field-of-view (FOV) cloud effects on passive microwave satellite estimates of LWP for nonprecipitating clouds. When broken cloudiness occurs within the instrument's large FOV (the effective instantaneous FOV is typically about 35 km), the instrument integrates across both clear and cloudy portions of the scene, which reduces the measured radiance as compared to an

overcast FOV. This reduction in radiance is often called the beam-filling effect, which leads to larger random errors and negative systematic errors in the retrievals. This effect is analogous to the beam-filling problem for passive microwave rainfall retrievals [e.g., *Chiu et al.*, 1990; *Short and North*, 1990], although that problem is far more complex because of the nonlinear relationship between brightness temperature and rain rate and the sometimes extreme spatial inhomogeneities of the rainfall within the FOV. *Miletta and Katsaros* [1995] used coincident data from the special sensor microwave imager (SSM/I) and the operational line scanner to identify the beam-filling problem for cloud LWP retrievals at 37 and 85.5 GHz. Since data sets of cloud LWP used in climate studies are typically averaged over a month and within large grid boxes (e.g., 2.5°), beam-filling is less of a problem [*Wielicki et al.*, 1995]. However, it is less clear whether this is necessarily true in specific regions that have persistently broken cloud conditions and for data averaged over shorter time intervals or finer spatial grid resolutions.

The aim of this study is to evaluate the effects of sub-FOV variable cloudiness on microwave retrievals of cloud LWP through detailed, simultaneous comparisons of the SR and microwave retrieval methods. Emphasis is placed on evaluating the uncertainties in the SSM/I cloud LWP retrievals resulting from the beam-filling error (BFE). The analyses are confined to nonprecipitating marine stratocumulus. For single-layered water clouds the SR method is expected to yield its most accurate estimate of cloud LWP. Precipitating clouds are excluded since the microwave retrievals are less reliable under those conditions. Because measurements near 35 GHz have been used historically for retrieving cloud LWP, we focus only on the BFE in 37-GHz observations from the SSM/I. The SR retrievals of cloud LWP are obtained from measurements of the new generation Geostationary Operational Environmental Satellite (GOES), which offers a unique opportunity to examine sub-FOV effects since cloud amount and cloud properties such as visible optical depth and effective radius can be determined within the SSM/I FOV.

2. Data and Analysis Methods

2.1. GOES 8 Imager

The imagers on the GOES 8 and GOES 9 represent a new series of GOES sensor with improved sensitivity, a new higher-resolution near-infrared channel, and enhanced scanning capabilities [*Menzel and Purdom*, 1994]. The GOES 8 was launched on April 13, 1994, and became operational on June 9, 1995. The imager has five channels whose spectral band-pass characteristics are indicated in Table 1. Channels 1, 2, 4, and 5 are very similar in spectral response to channels 1, 3, 4, 5, respectively, for the advanced very high resolution radiometer (AVHRR) on the NOAA polar orbiting satellites. The instantaneous spatial resolution of the imager at nadir is 1.0 km x 1.0 km for the visible channel and 4.0 km x 4.0 km for channels 2, 4, and 5. Because the resolution and spatial sampling of the various channels of the GOES 8 imager are not the same, it was necessary to first sample the visible data every other line and element to match the data from the full-resolution near-infrared and IR channels.

2.2. GOES 8 Imager Calibration

The visible channel (0.6 μm) on the GOES 8 imager has no onboard calibration. However, the remaining infrared channels

Table 1. Comparison of Spectral Bandpass Characteristics of GOES 8 Imager and NOAA 9 Advanced Very High Resolution Radiometer (AVHRR)

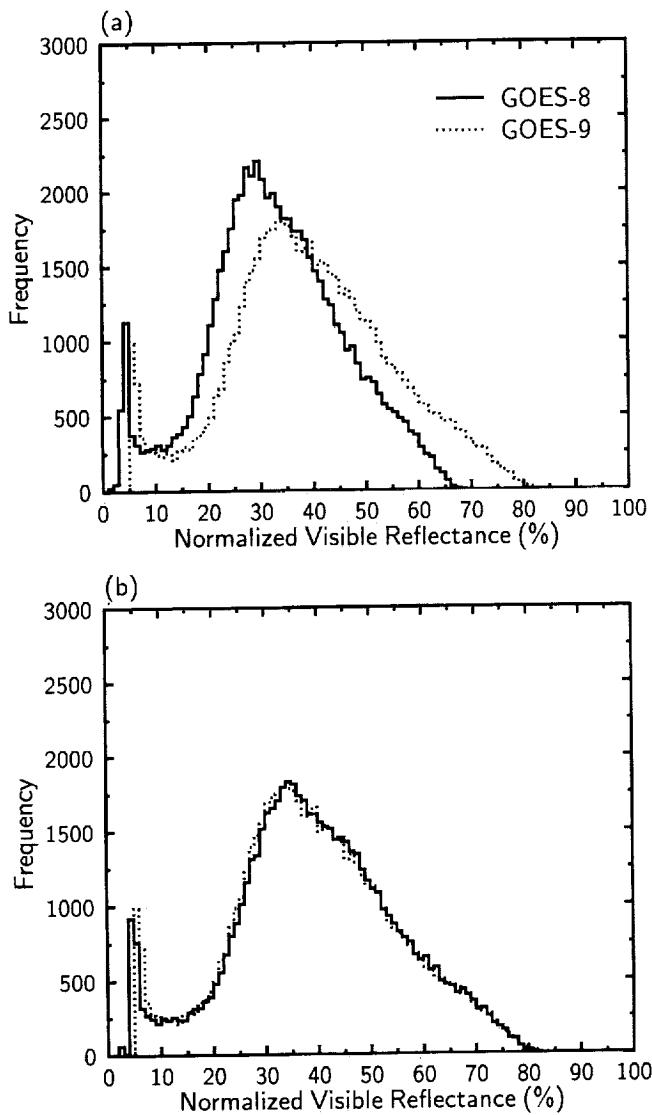| GOES 8 Imager		AVHRR	
Channel	Wavelength Range, μm	Channel	Wavelength Range, μm
1	0.52-0.72	1	0.58-0.68
-	-	2	0.725-1.1
2	3.78-4.03	3	3.55-3.93
3	6.47-7.02	-	-
4	10.2-11.2	4	10.3-11.3
5	11.5-12.5	5	11.5-12.5

have a reliable calibration scheme. There is some concern that the visible channel has degraded in sensitivity as compared to its prelaunch calibration. Current estimates of this degradation range between 15% and 20%, although 16% was a typical value as of July 1995 [*M. Weinreb, personal communication*, 1996]. Calibration is of critical importance to this study since we aim to compare the absolute magnitudes of the cloud LWP retrievals from the two methods. Therefore some quantitative estimate must be made of the apparent loss in sensitivity of the visible channel on the GOES 8 imager.

As a convenient and simple approach to this calibration problem, the visible measurements from the imagers on the GOES 9 and GOES 8 are intercalibrated. The GOES 9 imager may serve as an approximate calibration reference since it was launched only five months previous to the intercomparison, and because there is currently no evidence to suggest that its visible channel has undergone a similar degradation.

Several criteria are used in the selection of a case for intercomparison. First, simultaneous measurements are used to eliminate differences in the solar zenith angle and temporal changes in the cloud fields. Second, in order to minimize bidirectional effects it is essential to choose a region with a local noon Sun. Third, it is important to ensure that the scene viewed by each imager is at the same or nearly the same zenith angle. Another criterion to consider is the spatial variability of a scene [e.g., *Desormeaux et al.*, 1993], which can also affect the calibration procedure. This was not considered here since the scenes were nearly all overcast.

The GOES 8 and GOES 9 imagery selected for the intercalibration occurred at 1715 UTC November 1, 1995. At this time the GOES 9 was in a nonoperational mode and positioned at 90° W on the equator. GOES 8, on the other hand, was located at 75° W. The region between the two satellites (i.e., 75°-90° W) and extending from 10° to 20° S latitude was used in the comparison, which was done at the pixel level.

Figure 1a confirms a significant degradation in the visible channel of the GOES 8 imager as compared with the GOES 9 imager. The reflectances shown are normalized with respect to the cosine of the solar zenith angle. For the GOES 8 reflectance histogram to match the GOES 9 histogram, the reflectances need to be adjusted 20% higher (see Figure 1b). This is somewhat larger than earlier estimates of the degradation. Note that broken cloud fields probably cause the mismatch in the histograms for the lowest reflectances since these types of clouds were not eliminated from the comparison. GOES 8 visible reflectances were increased by 20% before being used in subsequent analyses.

Figure 1. Frequency histograms of GOES 8 imager versus GOES 9 imager channel 1 visible reflectances for 1715 UTC November 1, 1995, between 75° W and 90° W near South America showing (a) the degradation in GOES 8 and (b) after increasing the GOES 8 reflectances by 20%. Reflectances are normalized by the cosine of the solar zenith angle.

2.3. Collocation of Different Sensors

The collocation of the GOES 8 imager data with the SSM/I data is performed by simply finding the closest GOES 8 pixel that corresponds to the center of a given SSM/I pixel. Implementing this type of collocation procedure assumes the navigation of both satellite platforms is reasonably accurate. The accuracy in the position of the GOES 8 pixels is estimated to be about 2-4 km [Menzel and Purdom, 1994], while the geolocation for the SSM/I is less accurate, being within 5-10 km [Poe and Conway, 1990].

Once a GOES 8 pixel has been collocated with a SSM/I pixel, the surrounding GOES 8 pixels are then collected within the FOV of the SSM/I at 37 GHz. The shape of the SSM/I footprint is approximated as an ellipse. An average of about 80 GOES 8 pixels was found to occur within a given SSM/I footprint.

2.4. Cloud Detection

The identification of cloudy GOES 8 pixels is important in the retrieval of cloud optical properties and in determining the cloud amount within the microwave sensor's footprint. This study utilizes the "in-house" Clouds and Earth Radiant Energy System (CERES) Project cloud-masking scheme. This technique is based on a paired histogram approach [Baum et al., 1996] which uses global AVHRR images to identify 15 different classes (i.e., open water, Sun glint, water clouds, etc.). A total of 185 quantities using different combinations of the channels (i.e., channel ratios, channel differences, etc.) are calculated to develop an algorithm that separates the various classes based on the appropriate features. Note that although AVHRR measurements were used to develop this technique, the method was modified to accommodate the GOES 8 channels. The qualitative accuracy of the cloud mask was verified by visually inspecting the GOES 8 imagery.

3. Cloud Liquid Water Retrieval Methods

3.1 Solar Reflectance Method

The technique of retrieving the cloud optical depth and effective radius and hence the cloud LWP from reflected solar radiation measurements is described in detail by a number of authors [e.g., Nakajima and King, 1990, Han et al., 1994]; therefore only a short discussion will be given here. The principle of this technique is that solar reflectance measurements at nonabsorbing visible wavelengths are sensitive primarily to the optical depth of the cloud, while measurements at water-absorbing near-infrared wavelengths (excluding molecular absorption bands) respond mainly to changes in the effective size of the cloud drops.

The most common approach is to create a lookup table that contains the radiances for a range of cloud optical depths, cloud drop effective radii, and for different Sun-satellite viewing geometries. Here we use a similar approach but assume nadir-viewing conditions (most zenith angles were less than 35°). For a given pair of shortwave and near-infrared measurements and knowing the geometry, the optical depth and effective radius can be obtained simultaneously from the lookup table. Here the reflectance measurements are normalized by the cosine of the solar zenith angle. When the optical depth (τ) and effective radius (r_e) are known the cloud LWP (in units of grams per meter squared) simply follows from [Stephens, 1978]

$$LWP = \frac{2}{3} r_e \tau \tag{1}$$

where it is assumed the efficiency factor for the extinction of water drops at visible wavelengths is exactly 2 and the density of water is 10^3 kg m^{-3}.

The optical properties of the cloud drops and the phase functions are derived from Mie scattering theory. This information is used in a discrete ordinate radiative transfer model to compute the radiances at both wavelengths for the many different combinations of the cloud optical depth, effective radius, viewing geometry, and solar zenith angle. The reflectance of the ocean surface is set as 6% at 0.6 μm (channel 1) and 2.5% at 3.9 μm (channel 2), which are values for a smooth surface with an overhead Sun. Since the absorbing near-infrared wavelength also contains a component of emitted radiation, this effect is removed using the GOES 8 infrared window channel (11 μm) following standard techniques [e.g., Allen et al., 1990].

The lookup tables used in this study are based on the spectral response functions of the AVHRR onboard the NOAA 9 satellite,

(a)

(b)
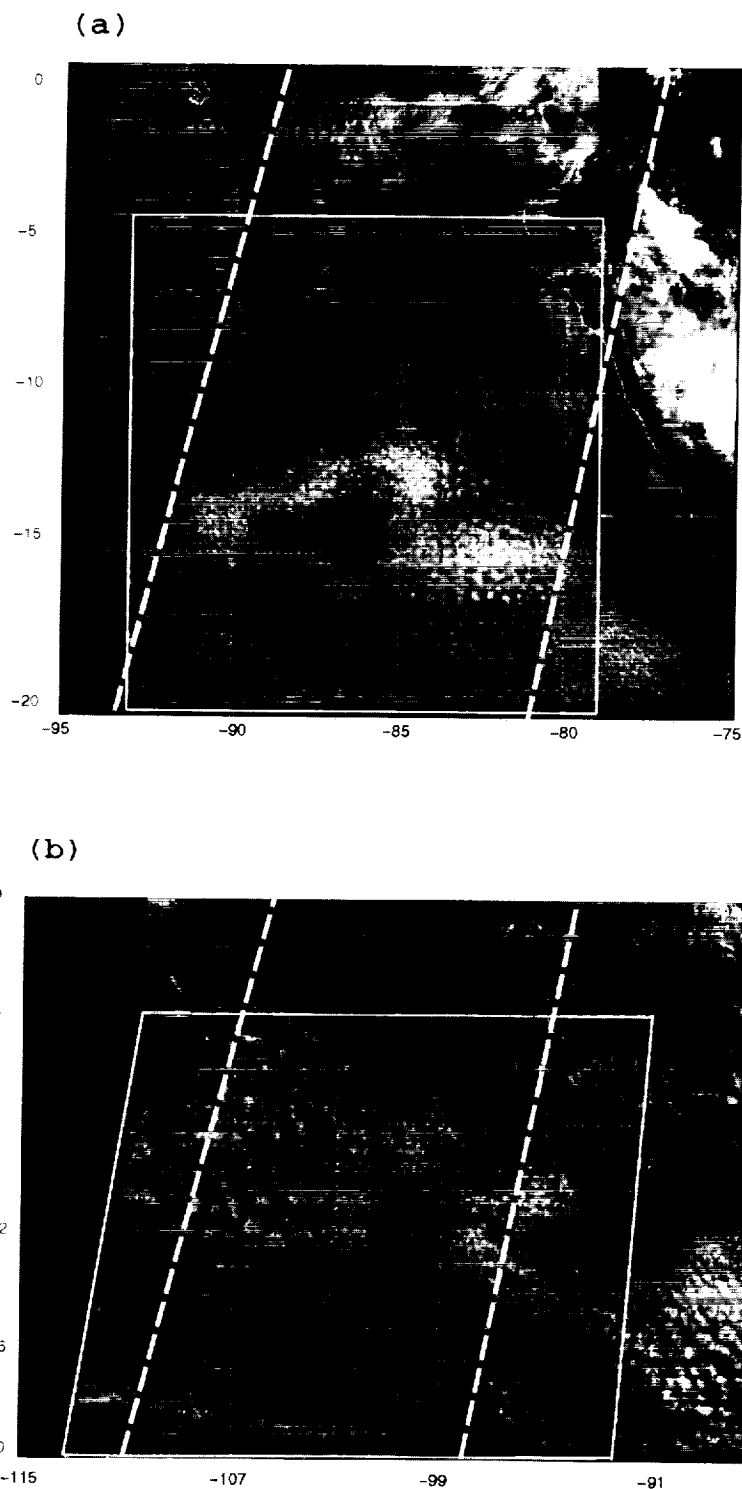
Figure 2. GOES 8 visible (channel 1) imagery for (a) 1523-1529 UTC, October 30, 1995 (case 1), and (b) 1653-1659 UTC, October 31, 1995 (case 2), depicting the case study regions (solid lines) and the edge of the Special Sensor Microwave Imager (SSM/I) swath (dashed lines).

since they were readily available. The use of AVHRR lookup tables for the GOES 8 imager channels can be justified on the grounds that the spectral responses of these two sensors are very close, as seen in Table 1. While the greatest difference in the response functions occurs for the near-infrared channels, these differences are expected to yield only small errors in the retrieved effective radii because of the large spectral overlap between the two sensors.

3.2. Microwave Methods

The cloud LWP retrievals from the microwave measurements are based on the method described by *Greenwald et al.* [1995]. It is a physical, iterative technique that uses the 19.35, 22.235, and 37 GHz channels of the SSM/I (refer to *Hollinger et al.* [1990] for a detailed description of the SSM/I). GOES 8 11-μm brightness temperatures are used in the retrieval model as an estimate

of the cloud temperature. An offset of 3 K is added to the 11-μm brightness temperatures to roughly account for atmospheric attenuation.

The retrievals initially indicated a positive systematic error in the cloud LWP of about 0.015-0.02 kg m^{-2}. This is not unexpected since regional systematic errors can sometimes occur in microwave retrievals of cloud LWP [Cober et al., 1996]. This error was corrected by calibrating the retrieval model in regions of clear sky using the approach of Greenwald et al. [1993]. While the magnitude of the correction is indeed very small, correctly calibrating the retrievals was a decidedly important factor in the beam-filling correction.

To take advantage of the higher-resolution 85.5 GHz measurements, further modifications to the Greenwald et al. [1995] method were required. Since the total optical depth of water vapor (τ_w) at this frequency is no longer directly proportional to the vertically integrated water vapor (W), it was necessary to deter-

mine an empirical relationship between τ_w and W. This was accomplished by using model calculations for a wide range of temperature and humidity profiles. The retrieval procedure consisted of inserting the value of W derived from the Greenwald et al. [1995] method (22.235 and 37 GHz) into an analytic brightness temperature equation [Greenwald et al., 1995] and then solving numerically for the cloud LWP.

Petty [1990] and Greenwald et al. [1993] have reported the errors in microwave retrievals of cloud LWP in detail. Presenting these errors as one number is perhaps inappropriate because the errors vary depending on the atmospheric conditions, the sea surface state, and the magnitude of the cloud LWP. For the conditions of our case studies and for a cloud LWP of 0.1 kg m^{-2}, the "random" errors can be expected to range from about 0.028 to 0.034 kg m^{-2}. This is not to be confused with "systematic" errors (e.g., one component of beam filling) that can contribute additional errors. However, if the systematic errors are known, these
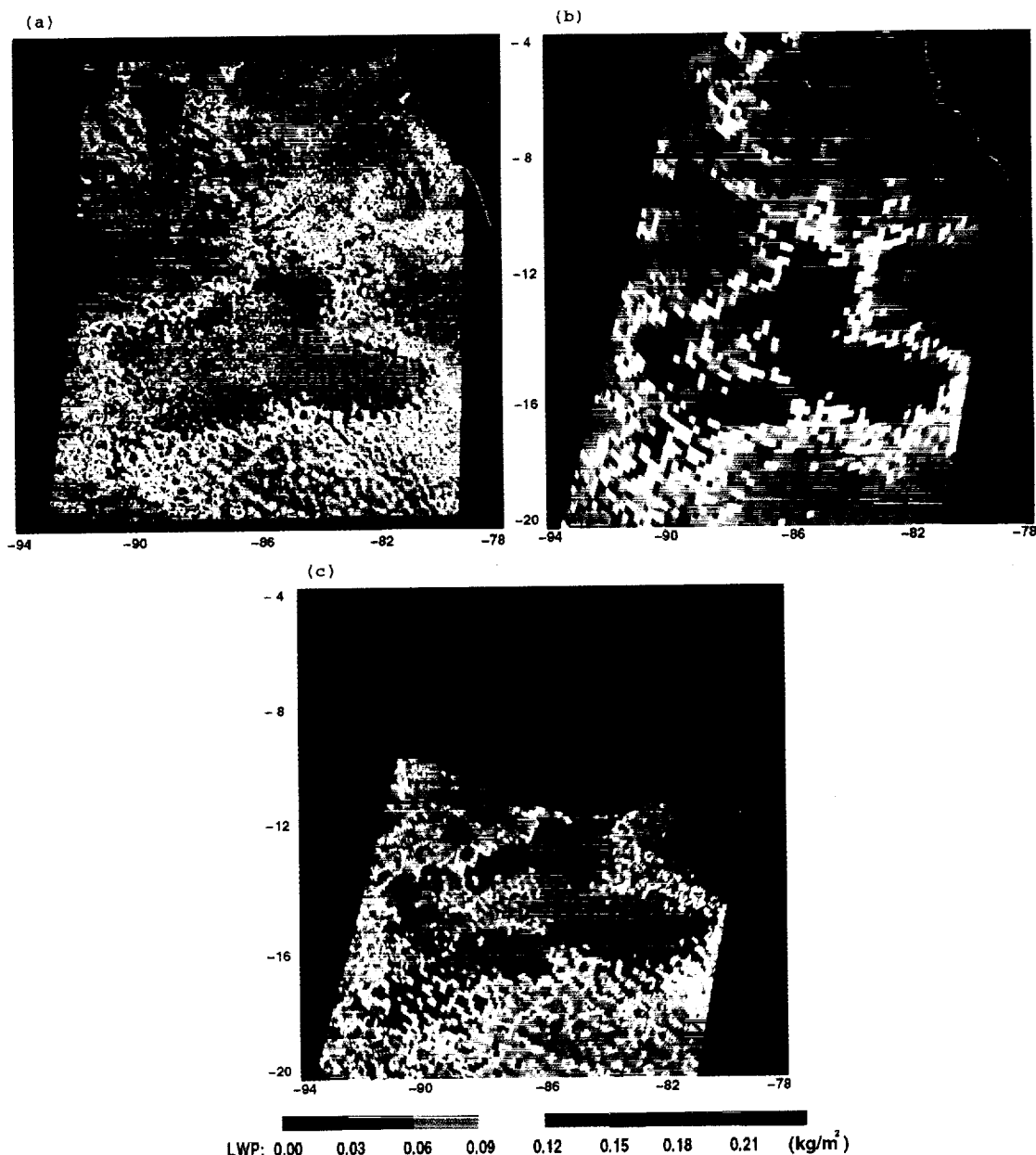
Plate 1. Spatial distribution of the retrievals of cloud LWP (kg m^{-2}) at full resolution for case 1 for (a) the solar reflectance method from the GOES 8 imager, and the SSM/I based on (b) vertical polarization 37 GHz measurements, and (c) horizontal polarization 85.5 GHz measurements.

error estimates are consistent with the study of *Cober et al.* [1996] who compared SSM/I retrievals of cloud LWP with aircraft measurements. For a cloud LWP of 0.2 kg m^{-2}, the random errors are dominated by uncertainties in the cloud temperature due to the strong dependence of the liquid water absorption coefficient on temperature [*Greenwald et al.,* 1993]. In this case, the errors are anticipated to be larger, from 0.035 to 0.043 kg m^{-2}.

4. Case Studies

At the end of October 1995 a very dense and persistent deck of marine stratocumulus formed off the coast of South America. Two cases were chosen during this time period. The GOES 8 visible (channel 1) imagery is shown in Figure 2. The first case (Figure 2a) at 1523-1529 UTC, October 30, includes a classic example of closed mesoscale cellular convection (MCC) [e.g., *Agee et al.,* 1973], which is thought to be driven by cloud-top radiative cooling in a weak stable boundary layer [*Shao and Randall,* 1996]. The solar zenith angles ranged from 25° to 37°. The edges of the swath for the Defense Meteorological Satellite Project (DMSP) F-10 satellite (dashed lines), which passed over the area at 1543-1547 UTC, are also shown.

The second case (Figure 2b), which occurs at 1653-1659 UTC, October 31, is farther west of the South American coast and is near a preferred region of development for open MCC where warm ocean currents and significant air-sea temperature gradients exist [*Agee et al.,* 1973]. It was chosen to contrast against the previous case since the stratocumuli are more "open" and variable in structure. Here the solar zenith angles were 18° to 35°. The DMSP F-10 overpass time was 1651-1656 UTC. All clouds in both case study regions were determined from the GOES 8 to have 11-μm brightness temperatures warmer than 280 K.

To test whether precipitation was occurring within these clouds, an emission-based method consisting of a normalized polarization index at 37 GHz was used [*Petty and Katsaros,* 1992]. The index (P_{37}) ranges from 0 to 1; values less than 0.8 are a reliable indicator of rainfall. For case 1, nearly all values of P_{37} were greater than 0.8. However, in case 2, a significant number of SSM/I FOVs had values less than 0.8 (as low as 0.57), which were concentrated along the "ribbon" of clouds running roughly east to west in the southernmost part of the sector (see Figure 2b). This result is confirmed by the SSM/I cloud LWP retrievals, which indicated fairly large LWP values ranging from 0.35 to 0.6 kg m^{-2}, whereas the GOES 8 retrievals had values typically less than 0.2 kg m^{-2}. These results suggest that either drizzle or light rainfall was likely occurring within this cloud system. Consequently, these clouds are excluded from the comparison.

5. Results

The spatial distribution of the cloud LWP derived from the SR and microwave methods for case 1 is shown in Plate 1. These results are presented at full resolution and remapped to a common projection. The GOES 8 cloud LWP field exhibits significant spatial variability and a large dynamic range, with values ranging from near 0.02 kg m^{-2} to more than 0.25 kg m^{-2}. The individual cells of the stratocumulus deck are also evident in Plate 1a (e.g., near 83° W and 16° S). They are characterized by decreasing values of cloud LWP from the center of the cells toward their edges, where narrow bands of downward motion reside.

From the perspective of the 37 GHz microwave observations (Plate 1b) the magnitude of the cloud LWP and the spatial patterns of the cloud fields resemble those derived from the SR method. The effects of beam filling are common throughout the region but are especially pronounced near 91° W and 19° S and in an area of highly broken cloudiness near 90° W and 10° S as seen from the GOES 8 cloud LWP field.

For comparison, the SSM/I retrievals using the higher-resolution 85.5 GHz measurements at horizontal polarization are also presented (Plate 1c). Retrievals are excluded for values of W beyond 32 kg m^{-2} due to the greatly reduced sensitivity of the 85.5 GHz brightness temperatures to changes in cloud LWP. Naturally, more details of the cloud field emerge, where the measurements begin to capture the cellular nature of the cloud system. However, the effects of beam filling still remain in many areas.
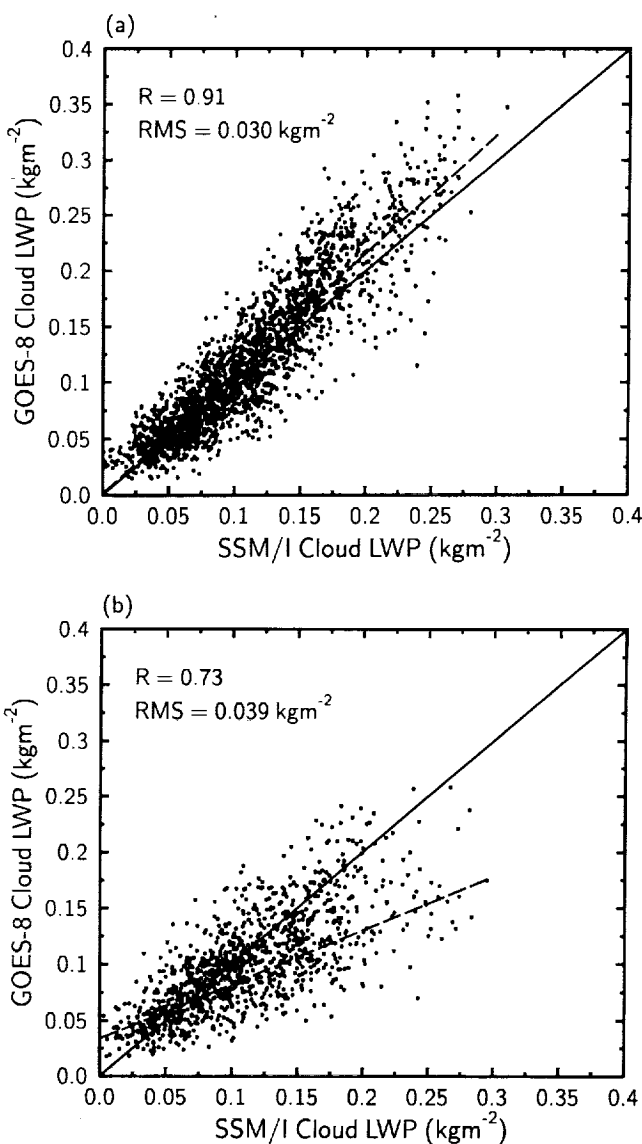
Figure 3. Comparisons of the GOES 8 cloud liquid water path (LWP) retrievals (kg m^{-2}) and the SSM/I retrievals for overcast SSM/I fields-of-views (FOVs) for (a) case 1 and (b) case 2. The RMS differences, lines from a least squares regression (dashed), linear correlation coefficients, and lines of perfect agreement are also indicated.
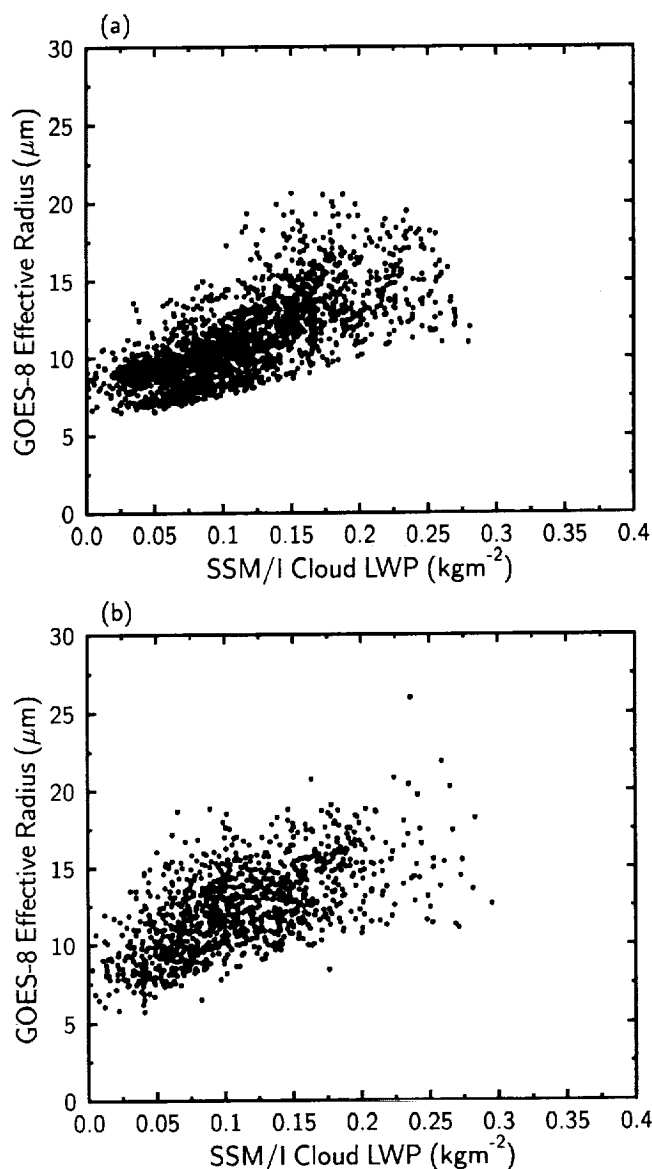
5.1 Overcast Conditions

For the special case of overcast conditions we expect the agreement between the two methods to be the best. This is confirmed in Figure 3, which shows a scatterplot of the GOES 8 cloud LWP (average within the SSM/I FOV) versus the SSM/I cloud LWP (37 GHz retrievals) for SSM/I FOVs in which the cloud amount is 100%. The correlation for case 1 (Figure 3a) is particularly high (0.91). These results provide added confidence in the magnitudes of the cloud LWP from both retrieval methods and in our calibration procedures.

Using the RMS difference as a gauge, these results further demonstrate that retrievals of cloud LWP from instantaneous 37 GHz measurements are in fact possible down to approximately 0.03 kg m^{-2} under overcast conditions, provided systematic errors have been accounted for. These results contradict those of *Lin and Rossow* [1994] who concluded that the 37 GHz measurements of the SSM/I were unable to detect cloud LWP below 0.05-0.07 kg m^{-2}.

There is also an indication of a slight bias in the results for case 1, especially for cloud LWP beyond 0.15 kg m^{-2}. We surmise that most of this bias is most likely caused by an underestimation in the SSM/I retrievals since merely the cloud top temperature is used in the retrieval model. As discussed earlier, an accurate determination of the cloud temperature becomes more crucial for larger LWP. A 3-5 K underestimation in the cloud temperature can account for most of the bias seen in Figure 3a. Further investigation into the specific cause(s) of this bias is difficult without additional information about the vertical temperature and humidity structure and the cloud base height.

In contrast, the results for case 2 (Figure 3b) are surprisingly different. The most obvious differences are the more significant bias (in a direction opposite to case 1) and the greater scatter. It is very unlikely that this bias is caused entirely by cloud temperature errors because a reduction in the cloud temperature of about 15 K would be needed for the results to agree. If we compare the mean standard deviation of the cloud LWP within the SSM/I FOV (σ_{LWP}) for these two cases (Table 2), we find that the mean sub-FOV variability in cloud LWP for case 2 is 20% higher than for case 1 even though the mean GOES 8 cloud LWP is about 17% lower.

These facts, along with the plane-parallel assumption used in the SR retrievals, suggest that a possible hypothesis for explain-

Figure 4. Comparisons of the effective radius (μm) derived from the GOES 8 and the SSM/I cloud LWP (kg m^{-2}) in overcast conditions for (a) case 1 and (b) case 2.

Table 2. Statistical Summary of GOES 8 and SSM/I Cloud Property Retrievals Under Overcast Conditions for Each Case

	Case 1	Case 2
GOES 8 cloud LWP, kg m^{-2}	0.12 ± 0.07	0.10 ± 0.04
SSM/I cloud LWP, kg m^{-2}	0.11 ± 0.06	0.11 ± 0.05
Optical depth	16 ± 7	12 ± 4
Effective radius, μm	11 ± 3	12 ± 3
σ_{LWP}, kg m^{-2}	0.040	0.048
σ_{LWP} (optical depth), kg m^{-2}	0.037	0.042
σ_{LWP} (effective radius), kg m^{-2}	0.010	0.015
N	2096	1092

The mean and standard deviation of the cloud liquid water path (LWP), optical depth, and effective radius retrievals are indicated. Also included is the mean standard deviation of the GOES 8 cloud LWP within the field-of-view (FOV) of the Special Sensor Microwave Imager (SSM/I) (σ_{LWP}) and separated into its components for variations due to optical depth and effective radius. N is the total number of points.

ing the differences might involve cloud structure variability. *Cahalan et al.* [1994] has shown for fractal marine stratocumulus clouds that the cloud structure reduces the visible albedo when compared to an idealized plane-parallel cloud. This bias is affected more by the variability of the liquid water and less by the mean liquid water. While the bias appears to be consistent with cloud variability, or even beam filling effects in the SR retrievals, its cause is not immediately known.

In terms of the mean statistics, the average GOES 8 and SSM/I cloud LWPs are within 10% of one another for both cases (Table 2). The optical depth and effective radius statistics are also consistent with previously published results for marine stratocumulus near southern California based on remote sensing from aircraft [*Nakajima et al.*, 1991] (Note that Nakajima et al. did not provide mean values of these quantities; however, the probability density functions of optical depth and r_e for their July 7 and July 13 cases were very similar to those of this study). The

mean optical depth is 25% lower for case 2 relative to case 1; however, with respect to the cloud LWP, this is partly compensated for by the 14% larger mean effective radius for case 2.

The sub-FOV variability of the cloud LWP can be examined further by separating the variability into its two components. Using (1), the sub-FOV standard deviation in cloud LWP due to variations in optical depth and effective radii can be defined by

$$\left(\sigma_{LWP}\right)_\tau = \frac{\partial\,LWP}{\partial\tau}\sigma_\tau \approx \frac{2r_e\sigma_\tau}{3} \qquad (2)$$

$$\left(\sigma_{LWP}\right)_{r_e} = \frac{\partial\,LWP}{\partial r_e}\sigma_{r_e} \approx \frac{2\tau\sigma_{r_e}}{3} \qquad (3)$$

where σ_τ and σ_{r_e} are the sub-FOV standard deviations for the optical depth and effective radius, respectively. Note that the values of r_e and τ in (2) and (3) are the mean quantities within the SSM/I FOV. Not unexpectedly, as shown in Table 2, the variation in the cloud LWP is largely determined by variations in optical depth for both cases, where the variation is about 3 times that due to changes in effective radius.

Additional information about the bulk microphysical characteristics of the cloud systems can be gleaned from a correlation between the effective radius estimated from GOES 8 and the cloud LWP obtained from the SSM/I, both of which are independently derived. The comparisons (Figure 4) reveal a weak, positive (yet statistically significant) correlation between these quantities. These results are in good agreement with the remote sensing observations of *Nakajima et al.* [1991] for Californian marine stratocumulus and with the in situ observations of primarily marine stratocumulus summarized in that study.

An alternative (and far more indirect) way of determining the effective radius is to use the SSM/I cloud LWP and the visible optical depth from GOES 8 and calculate the effective radius from (1). Figure 5 illustrates the inferred effective radii based on this method versus the effective radii derived from GOES 8. For Case 1 there is reasonable agreement between the two estimates, but a small bias exists. On the other hand, the agreement for case 2 is poor, often overestimating the effective radius by 10-15 μm.

Another estimate of the errors in these r_e retrievals can be derived through an error propagation analysis. From (1) the random error in r_e can be written as

$$\sigma_{r_e} \approx \frac{3}{2}\left[\left(\frac{\sigma_{LWP}}{\tau}\right)^2 + \left(\frac{-LWP\sigma_\tau}{\tau^2}\right)^2\right]^{\frac{1}{2}}$$

where σ_{LWP} is the uncertainty in the SSM/I retrievals (determined from the error analysis of *Greenwald et al.* [1993]); the other variables are as previously defined in (2) and (3). This analysis shows that the mean random errors in the r_e retrievals are 5.4 μm and 8.4 μm for cases 1 and 2, respectively.

On the basis of the comparisons and the error analysis, this method appears to be of limited use, even under overcast conditions. While in special cases it might provide reasonable estimates of r_e when averaged over a region, it is sometimes subject to large errors and is very sensitive to the relative biases between the retrieved visible optical depth and the microwave cloud LWP. For cases in which broken cloudiness exists within the SSM/I FOV, there are expected to be even larger systematic errors in these estimates.

5.2 Nonovercast Cloud Conditions

The next step is to quantify the BFEs in the retrieval of cloud LWP from SSM/I measurements under conditions that are most
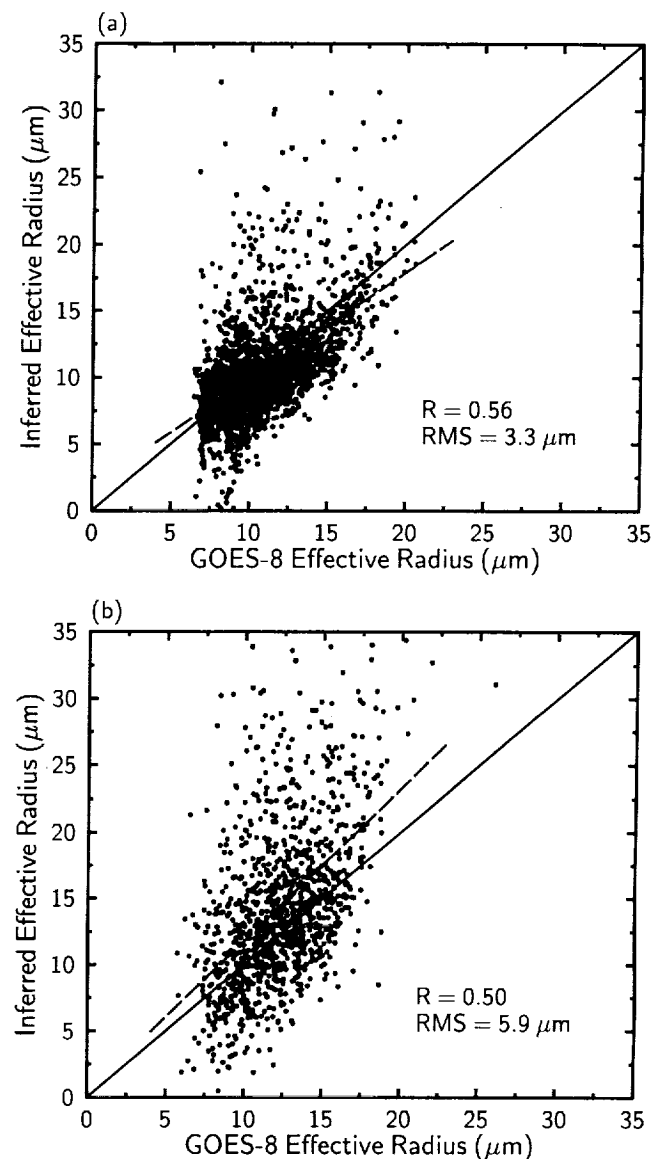

Figure 5. Effective radius (μm) inferred from a combination of the GOES 8 visible optical depth retrievals and the SSM/I cloud LWP retrievals versus the GOES 8 effective radius retrievals in overcast conditions for (a) case 1 and (b) case 2. The RMS difference, lines from a least squares regression (dashed), linear correlation coefficient, and lines of perfect agreement are also shown.

likely to be encountered within the FOV, i.e., partly to mostly cloudy. For each case, the cloud LWP observations for both the GOES 8 and the SSM/I were collected into cloud amount bins (10% interval) of the cloud cover within the FOV of the SSM/I (excluding cloud amounts of 0% and 100%). The results are presented in Figure 6. The standard deviation of the data in each bin is indicated as the shaded region. Also shown for reference is the approximate noise level (or minimum error) of the microwave retrievals (0.02 kg m^{-2}) as determined from the clear sky retrievals.

The decrease in the SSM/I cloud LWP with decreasing cloud amount (Figures 6a and 6c) is the characteristic beam-filling effect. Since the optical depth of the clouds is very small at 37 GHz (usually less than 0.1), the decrease in cloud LWP is closely linear. This behavior is not caused simply by a decrease in the LWP
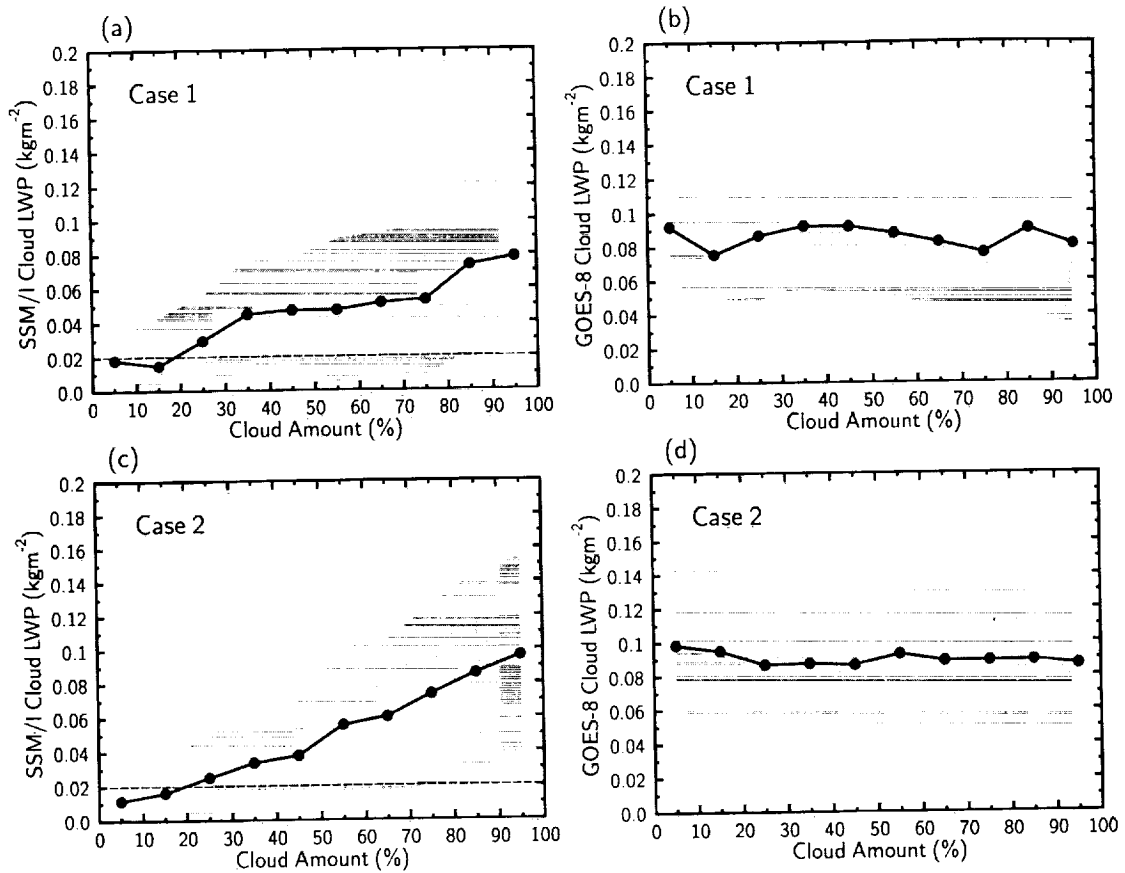
Figure 6. SSM/I cloud LWP retrievals versus cloud amount (%) within the SSM/I FOV for (a) case 1 and (c) case 2. The corresponding relationships for cases 1 and 2 for the GOES 8 cloud LWP retrievals are shown in Figures 6b and 6d, respectively. Also indicated is the standard deviation of the data in each bin (gray shading) and the noise level of the SSM/I retrievals (dashed lines).

of the clouds as the cloud field becomes more broken since the GOES 8 results (Figures 6b and 6d) show that the cloud LWP is nearly independent of cloud cover within the SSM/I FOV.

The mean statistics for the retrievals under broken cloud conditions are compiled in Table 3. In terms of the average systematic BFEs the cloud LWP is underestimated by 27% for case 1 in comparison to the GOES 8 retrievals and 16% for case 2. The respective average cloud amounts are 73% and 72%. Also, the average sub-FOV standard deviation of the cloud LWP is relatively larger than the overcast cases, and the contribution to the standard deviation from variations in the effective radius is also more significant.

With information about the cloud amount within the SSM/I FOV it is possible to correct for the systematic component of the BFE. Here we propose a simple first-order correction by dividing the cloud LWP by the cloud amount since there is a nearly linear relationship between the SSM/I cloud LWP and cloud amount. Because of the near-linearity in the radiative transfer, scaling the cloud LWP by the cloud amount is essentially equivalent to linearly weighting the clear sky and cloudy components of the brightness temperatures within the FOV. The implicit assumption in this correction is that the LWP of each of the cloud elements within the FOV is the same. As seen by the large sub-FOV standard deviations (about 55% of the mean value) in Table 3, this is clearly not the case. Presumably, the cloud LWP sub-FOV variability will also play a role in the beam-filling correction, although it is not considered here.

The same analysis as before (Figure 6) was also done for the corrected SSM/I cloud LWP retrievals, and the results are shown in Figure 7. This simple correction works well for values of the cloud amount greater than about 20-25% but appears to break down for smaller values. The cloud LWP is overestimated by a factor of 2 or more for the lowest cloud amount category and the standard deviation increases dramatically. This behavior is the result of the average cloud LWP retrievals falling below the noise threshold of the observations, which occurs for cloud amounts below about 20-25% (see Figures 6a and 6c). Thus it can be concluded that 37 GHz measurements from the SSM/I are

Table 3. Same as Table 1 But for Nonovercast Cases and Including Mean Cloudiness

	Case 1	Case 2
GOES 8 cloud LWP, kg m^{-2}	0.085 ± 0.044	0.090 ± 0.040
SSM/I cloud LWP, kg m^{-2}	0.062 ± 0.054	0.075 ± 0.059
Optical depth	6.8 ± 2.8	7.3 ± 2.5
Effective radius, μm	19 ± 7	19 ± 6
σ_{LWP}, kg m^{-2}	0.047	0.051
σ_{LWP} (optical depth) kg m^{-2}	0.041	0.045
σ_{LWP} (effective radius) kg m^{-2}	0.021	0.023
Mean cloudiness, %	73	72
N	894	2611
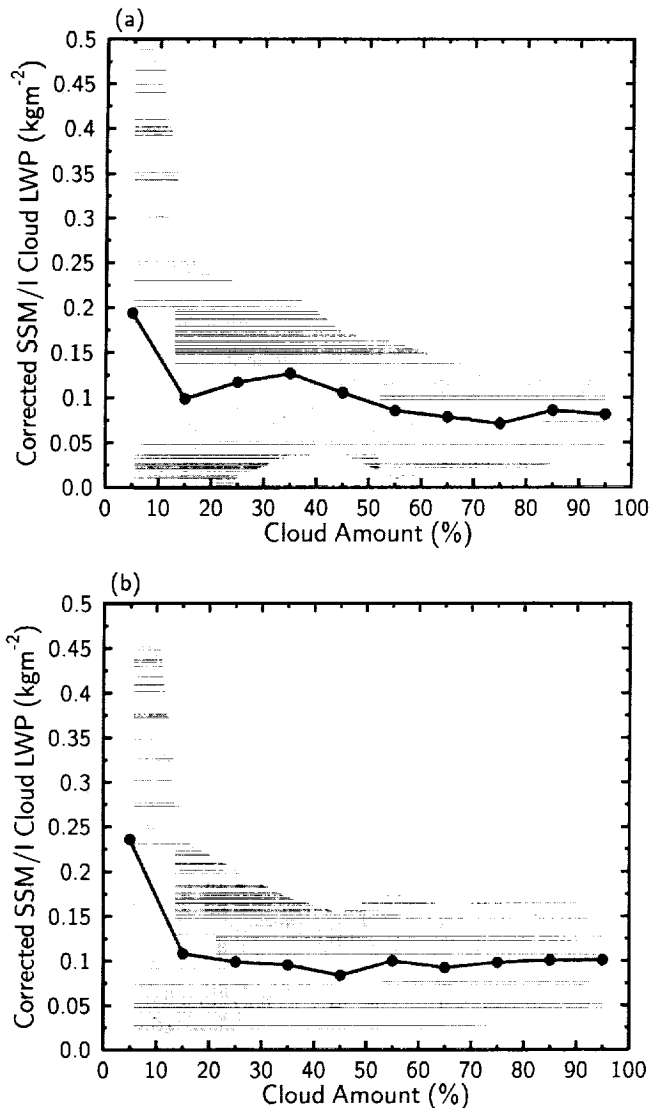
Figure 7. Comparisons of the SSM/I cloud LWP retrievals corrected for beam filling versus cloud amount (%) for (a) case 1 and (b) case 2. Gray shading indicates the standard deviation within each bin.

These results provide only a crude measure of the uncertainties that result from the first-order beam-filling correction. Nevertheless, the larger random errors in the SSM/I retrievals are likely attributed to the variation of cloud LWP within the SSM/I FOV. More extreme outliers are also evident, which is likely due to errors in the satellite navigation or possible errors in the cloud detection algorithm. In terms of the mean cloud LWP the SR and microwave retrievals gave 0.095 kg m^{-2} and 0.11 kg m^{-2}, respectively, for case 1 and 0.093 kg m^{-2} and 0.11 kg m^{-2} for case 2.

6. Conclusions

Comparisons between the cloud LWP derived from two independent techniques, the solar reflectance and passive microwave methods, have been conducted for marine clouds using measurements from the GOES 8 imager and the SSM/I in order to quantify the effects of beam filling on the 37 GHz retrievals. Two case studies were selected for nonprecipitating stratocumulus off
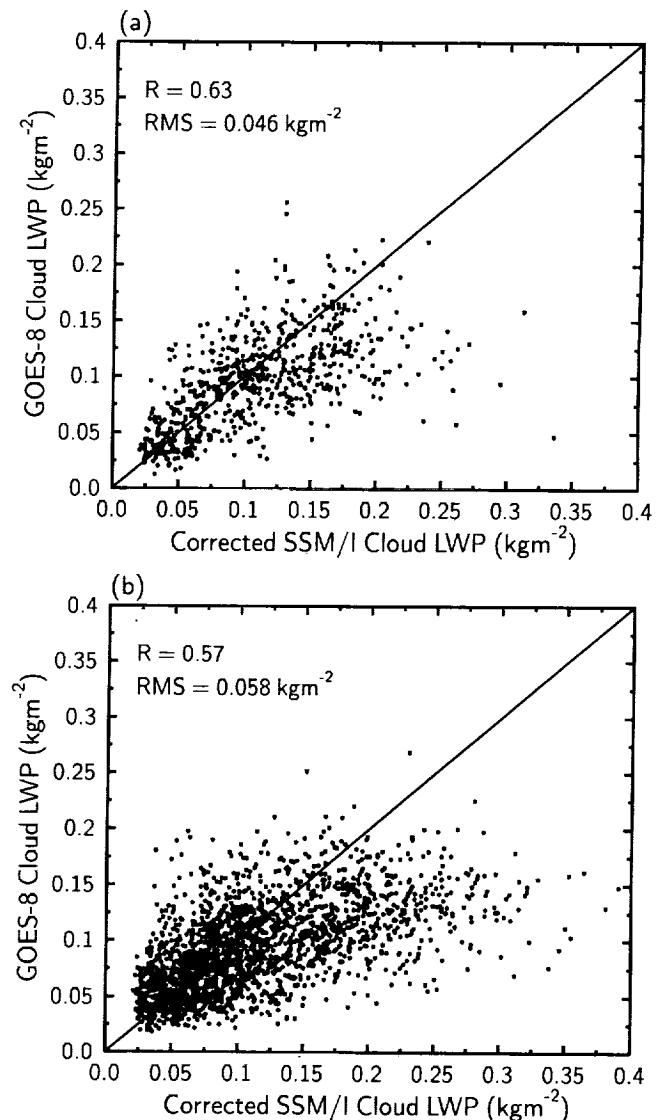
not useful for retrieving cloud LWP if the cloud amount within the FOV is less than about 25%. Use of the 85.5 GHz measurements may be necessary in these situations, as they are theoretically more sensitive to changes in cloud LWP. However, we stress that this type of beam-filling correction may be inappropriate for the 85.5 GHz retrievals since the relationship between the SSM/I cloud LWP and the cloud amount is expected to be somewhat nonlinear [*Miletta and Katsaros*, 1995].

Although the systematic component of the BFE can be largely accounted for, the cloud LWP retrievals also acquire additional random errors. To investigate this in more detail, we show in Figure 8 a scatterplot of the GOES 8 cloud LWP versus the corrected SSM/I cloud LWP but only for cloud amounts beyond 25% and SSM/I retrievals greater than 0.02 kg m^{-2}. The linear correlation is weaker and the scatter is greater than for the overcast results (compare Figure 3), with the RMS differences increasing to 0.046 kg m^{-2} for case 1 and 0.058 kg m^{-2} for case 2. Also, the results for case 2 (Figure 8b) indicate that some significant biases remain for larger cloud LWP.

Figure 8. Scatter diagram of the data used in Figure 7 for (a) case 1 and (b) case 2 but excluding cloud amounts less than 25% and SSM/I retrievals below 0.02 kg m^{-2}. The linear correlation coefficients, RMS differences, and lines of perfect agreement are shown.

the coast of South America for October 30-31, 1995. Measurements from the 0.6-μm and 3.9-μm channels of the GOES 8 were used to retrieve simultaneously both the optical depth and the effective radius of the clouds. The effective radius retrievals were necessary to minimize errors resulting from changes in the size of the droplets in the SR retrievals of cloud LWP.

The use of coincident, high-resolution visible and/or infrared measurements is essential in the interpretation of passive microwave observations of cloud LWP, as similarly determined by *Miletta and Katsaros* [1995]. Important in this analysis is the collocation of the different measurements while at the same time maintaining their full resolution. This allowed for an accurate determination of the degree of cloudiness within the FOV of the SSM/I, which would not have been possible otherwise.

For retrievals in which the SSM/I FOV was completely overcast, it was found that the two methods compared favorably for stratocumulus composed of closed MCC (RMS difference of 0.030 kg m^{-2}). For open MCC, the SR retrievals were generally biased lower than the microwave retrievals (the RMS difference was 0.039 kg m^{-2}). These differences may be related, in part, to variations in cloud structure, although additional work is needed to confirm this hypothesis. Further comparisons of GOES 8 retrievals of the effective radius and the SSM/I cloud LWP retrievals revealed an increase in effective radius with increasing cloud LWP, consistent with in situ measurements and other remote sensing studies [e.g., *Nakajima et al.*, 1991].

Another key result is that measurements at 37 GHz are clearly more responsive to small cloud LWP than previously reported [e.g., *Weng and Grody*, 1994; *Lin and Rossow*, 1994; *Miletta and Katsaros*, 1995]. This study differentiates between overcast and partially cloud-filled FOVs when addressing the sensitivity of these measurements to cloud LWP. As long as systematic errors in the retrievals are known, reasonable estimates of cloud LWP can be obtained for thin, overcast clouds with LWP as small as approximately 0.03 kg m^{-2}, consistent with the validation study of *Cober et al.* [1996].

The relationship between 37-GHz retrievals of cloud LWP from the SSM/I and sub-FOV cloud amount is determined to be nearly linear. Thus, the systematic errors caused by beam filling in SSM/I 37-GHz observations of cloud LWP can be largely accounted for by applying a simple linear correction based on knowledge of the sub-FOV cloud amount. When compared to the SR retrievals, the corrected microwave retrievals have larger RMS differences of 0.046-0.058 kg m^{-2}, which is mainly the result of sub-FOV variations in cloud LWP. Without the correction, however, one can expect, on the average, low biases in the microwave retrievals of about 22% from beam filling when the average cloudiness is 73%. These errors are similar in magnitude to the average random errors in the retrievals ($\approx$31%). However, for individual FOVs and for less regional cloudiness, the BFEs often exceed the random retrieval errors. Furthermore, the correction is not useful when the retrieved cloud LWP falls below the noise level of the measurements and for cloud amounts less than about 25% within the FOV. The beam-filling correction proposed here is strictly valid for SSM/I FOVs containing only water clouds, although it may be applied without a great loss in accuracy if there is not significant high-level cloudiness within the FOV.

Beam-filling effects will likely have an immediate and serious impact on studies that use instantaneous microwave satellite measurements. Knowledge of the BFEs should be very important for verification studies in which the satellite retrievals are compared directly to ground-based or in situ measurements. Beam-

filling will also have an impact on the analysis and interpretation of weather systems, including cloud classification techniques that rely on estimates of the cloud LWP [e.g., *Sheu et al.*, 1997]. Retrievals of near-surface wind speed from passive microwave measurements under broken cloudiness may suffer additional systematic errors since the impact of clouds on the brightness temperatures will be underestimated. Moreover, these effects will likely play a role in the future prospect of assimilating satellite retrievals of cloud LWP into weather forecast models.

References

Agee, E. M., T. S. Chen, and K. E. Dowell, A review of mesoscale cellar convection, *Bull. Am. Meteorol. Soc.*, *54*, 1004-1012, 1973.

Allen, R. C., Jr., P. A. Durkee, and C. H. Wash, Snow/cloud discrimination with multispectral satellite measurements, *J. Appl. Meteorol.*, *29*, 994-1004, 1990.

Baum, B.A., et al., Imager clear-sky determination and cloud detection, in *Clouds and the Earth's Radiant Energy System (CERES) Algorithm Theoretical Basis Document*, subsyst. 4.1, release 2.1, NASA Langley, Hampton, VA, 44 pp., 1996.

Cahalan, R. F., W. Ridgway, W. J. Wiscombe, T. L. Bell, and J. B. Snider, The albedo of fractal stratocumulus clouds, *J. Atmos. Sci.*, *51*, 2434-2455, 1994.

Chiu, L. S., G. R. North, D. A. Short, and A. McConnel, Rain estimation from satellites: Effect of finite field of view, *J. Geophys. Res.*, *95*, 2177-2185, 1990.

Cober, S. G., A. Tremblay, and G. A. Isaac, Comparisons of SSM/I liquid water paths with aircraft measurements, *J. Appl. Meteorol.*, *35*, 503-519, 1996.

Desormeaux, Y., W. B. Rossow, C. L. Brest, and G. G. Campbell, Normalization and calibration of geostationary satellite radiances for the International Satellite Cloud Climatology Project, *J. Atmos. Ocean. Technol.*, *10*, 304-325, 1993.

Greenwald, T. J., G. L. Stephens, T. H. Vonder Haar, and D. L. Jackson, A physical retrieval of cloud liquid water over the global oceans using special sensor microwave/imager (SSM/I) observations, *J. Geophys. Res.*, *98*, 18,471-18,488, 1993.

Greenwald, T. J., G. L. Stephens, S. A. Christopher, and T. H. Vonder Haar, Observations of the global characteristics and regional radiative effects of marine cloud liquid water, *J. Clim.*, *8*, 2928-2946, 1995.

Greenwald, T. J., C. L. Combs, A. S. Jones, D. L. Randel, and T. H. Vonder Haar, Further developments in estimating cloud liquid water over land using microwave and infrared satellite measurements, *J Appl. Meteorol.*, *36*, 389-405, 1997.

Han, Q., W. B. Rossow, and A. A. Lacis, Near-global survey of effective droplet radii in liquid water clouds using ISCCP data, *J. Clim.*, *7*, 465-497, 1994.

Hollinger, J. L. Peirce, and G. A. Poe, SSM/I instrument evaluation, *IEEE Trans. Geosci. Remote Sens.*, *GE-28*, 781-791, 1990.

Jones, A.S., and T.H. Vonder Haar, Passive microwave remote sensing of cloud liquid water over land regions, *J. Geophys. Res.*, *95*, 16,673-16,683, 1990.

Lin, B., and W. B. Rossow, Observations of cloud liquid water path over oceans: Optical and microwave remote sensing methods, *J. Geophys. Res.*, *99*, 20,907-20,927, 1994.

Lojou, J.-Y., R. Frouin, and R. Bernard, Comparison of Nimbus-7 SMMR and GOES 1 VISSR atmospheric liquid water content, *J. Appl. Meteorol.*, *30*, 187-198, 1991.

Menzel, P. W., and J. F. W. Purdom, Introducing GOES I: The first of a new generation of geostationary operational environmental satellites, *Bull. Am. Meteorol. Soc.*, *75*, 757-781, 1994.

Miletta, J., and K. B. Katsaros, Using coincident multispectral satellite data to assess the accuracy of SSMI liquid water path measurements, *J. Geophys. Res.*, *100*, 16,333-16,339, 1995.

Nakajima, T., and M. D. King, Determination of the optical thickness and ef-

fective particle radius of clouds from reflected solar radiation measurements, I, Theory, *J. Atmos. Sci.*, *47*, 1878-1893, 1990.

Nakajima, T., M. D. King, J. D. Spinhirne, and L. F. Radke, Determination of the optical thickness and effective particle radius of clouds from reflected solar radiation measurements, II, Marine stratocumulus observations, *J. Atmos. Sci.*, *48*, 728-750, 1991.

Petty, G. W., On the response of the Special Sensor Microwave/Imager on the marine environment—Implications for atmospheric parameter retrievals, Ph.D. dissertation, Univ. of Wash., 291 pp., Seattle, 1990.

Petty, G. W., and K. B. Katsaros, Nimbus-7 SMMR precipitation observations calibrated against surface radar during TAMEX, *J. Appl. Meteorol.*, *31*, 489-505, 1992.

Poe, G. A., and R. W. Conway, A study of the geolocation errors of the Special Sensor Microwave / Imager (SSM/I), *IEEE Trans. Geosci. Remote Sens.*, *28*, 791-799, 1990.

Shao, Q. and D. A. Randall, Closed mesoscale cellar convection driven by cloud-top radiative cooling, *J. Atmos. Sci.*, *53*, 2144-2165, 1996.

Sheu, R.-S., J. A. Curry, and G. Liu, Vertical stratification of tropical cloud properties as determined from satellite, *J. Geophys. Res.*, *102*, 4231-4245, 1997.

Short, D. A., and G. R. North, The beam filling error in Nimbus-5 ESMR observations of gate rainfall, *J. Geophys. Res.*, *95*, 2187-2193, 1990.

Stephens, G. L., Radiation profiles in extended water clouds, II, Parameterization schemes, *J. Atmos. Sci.*, *35*, 2123-2132, 1978.

Weng, F., and N. C. Grody, Retrieval of cloud liquid water using the special sensor microwave imager (SSM/I), *J. Geophys. Res.*, *99*, 25,535-25,551, 1994.

Wielicki, B. A., R. D. Cess, M. D. King, D. A. Randall, and E. F. Harrison, Mission to planet earth: Role of clouds and radiation in climate, *Bull. Am. Meteorol. Soc.*, *76*, 2125-2153, 1995.

J. Chou and S.A. Christopher (corresponding author), Institute of Atmospheric Sciences, South Dakota School of Mines and Technology, 501 East St. Joseph Street, Rapid City, SD 57701-3995.

T.J. Greenwald, Cooperative Institute for Research in the Atmosphere, Colorado State University, Fort Collins, CO 80523.